

## ERRORS AND UNCERTAINTIES IN PROBABILISTIC ENGINEERING ANALYSIS

Ben H. Thacker\*, David S. Riha†, Harry R. Millwater‡, and Michael P. Enright†  
 Southwest Research Institute  
 San Antonio, Texas

### Abstract

The developing field of probabilistic design has matured to the point where several classes of analysis methods have been proven to be useful for engineering analysis of large high fidelity structures with uncertain parameters. However, several barriers still stand in the way of widespread acceptance of probabilistic methods into the design practice. These include lack of data for characterizing probabilistic inputs, lack of understanding of analysis methodologies and associated limitations, lack of commercially available tools for performing probabilistic analysis, and lack of verification and validation examples. As a first step towards developing more computationally robust tools for performing probabilistic analysis and improving user understanding of analysis assumptions and limitations, this paper identifies the various types of error that can be encountered when performing probabilistic analysis and offers some suggestions for mitigating or eliminating them from the analysis.

### Introduction

The need to decrease reliance on testing and recent advances in high performance computing and has led to high fidelity numerical simulation becoming more widely used to predict the behavior and response of complex engineered systems. The reliability, robustness, or safety of some of these problems are high-consequence systems that cannot ever be tested. Examples include the science-based certification of the Nations aging nuclear stockpile, design of high-performance aircraft and aerospace engines and airframes, and explosive damage to commercial property such as buildings, aircraft and factories. Increased competitiveness to reduce costs and time-to-market is also driving the need for high-confidence simulation-based design.

Regardless of the need, the credibility of computational results is of great current concern to both the decision makers and those who are affected by the decisions that are based on these predictions because of the staggeringly high potential cost of failure. As a result, it is becoming widely accepted that proven processes and tools are needed to identify, manage and possibly mitigate the effects of errors and uncertainties that result from the process of representing a physical system with a numerical simulation. In general, uncertainty quantification

(UQ) methods (probabilistic, possibilistic, etc.) are used to deal with uncertainties, whereas procedural methods, primarily verification and validation (V&V), are used to identify and eliminate errors in the computational simulation. Organized efforts are underway to clearly define the V&V process for computational fluid and solid mechanics problems.<sup>1</sup> Similar such efforts are needed for UQ problems.

The paper discusses the relationship between error and uncertainty in a probabilistic analysis, identifies the various sources of uncertainty and what analysis methods may be appropriate, identifies the various sources of error associated with several of the popular probabilistic analysis methods, and suggests an approach for reducing or eliminating error to an acceptable level. Several example problems are used to illustrate the classifications, problems, and approaches suggested in the paper.

### Probabilistic analysis methods

All probabilistic analysis methods are approximate. Monte Carlo simulation, which is oftentimes referred to as the “exact” solution, is actually approximate because a finite number of samples is always used. Thus, the nature of the approximation is one of “lack of data,” which can be reduced by increasing the number of samples. However, for large-scale high fidelity problems, the inefficiency of Monte Carlo renders it impractical for use.

Many “efficient” methods have been devised to alleviate the need for Monte Carlo simulation. These methods include the first and second-order reliability method<sup>2</sup> (FORM and SORM), the advanced mean value family of methods<sup>3</sup> (AMV), and the response surface method<sup>4</sup> (RSM). These methods replace the original deterministic model with a computationally efficient analytical model in order to speed up the analysis. In many cases, unfortunately, the error associated with this approximation is not quantified by the method, which leaves the accuracy of the result in question. More efficient sampling techniques, such as adaptive importance sampling<sup>5</sup> (AIS), show great promise for solving complex problems in an efficient manner. However, most importance sampling methods rely on the quality of the analytical approximation to the original model. Furthermore, in all cases, since numerical iterations are required, convergence error will also exist.

\* Principal Engineer, Senior Member AIAA

† Senior Research Engineer, Member AIAA

‡ Principal Engineer, Member AIAA

Copyright © 2001 Southwest Research Institute.

Published by the American Institute of Aeronautics and Astronautics, Inc. with permission.

The cornerstone of many efficient probabilistic analysis methods is locating the most probable point (MPP) with a minimum number of model (function) evaluations. This is usually accomplished using an optimization algorithm that locates the minimum distance,  $\beta$ , from the failure surface to the origin in a transformed probability ( $u$ ) space as shown in Figure 1. Many standard optimization algorithms are available to perform this task such as the modified method of feasible directions (MMFD), sequential linear programming (SLP), and sequential quadratic programming<sup>6</sup> (SQP). Some have also been developed specifically for probabilistic analysis such as the Rackwitz-Feissler method<sup>7</sup> (RF), which is widely used in structural reliability analysis. However, locating the MPP may be difficult or impossible when highly nonlinear or discontinuous response functions, multiple MPP's, or problems containing random variables with bounded distributions (e.g., uniform) are present. Details on the probabilistic methods used in the paper can be found in Ref. 8; optimizations methods are described in Ref. 6.

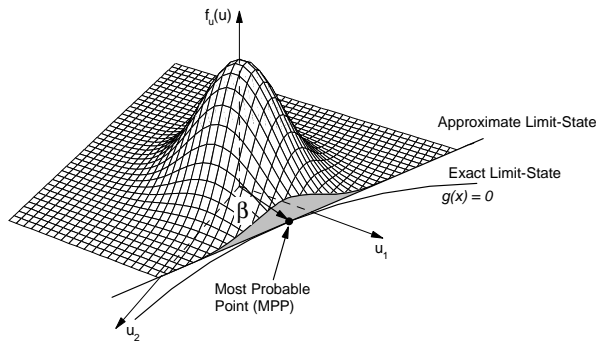


**Figure 1. Joint probability density function (jpdf), exact and approximate limit-state, and most probable point (MPP) for two random variables in transformed ( $u$ ) space.**

### Source and classification of Error in probabilistic analysis

Errors in computed probabilistic results will always be present due to characteristics of the numerical solution process employed, lack of data, and human error. As will be discussed, our opinion is that all forms of error can be reduced through V&V of the probabilistic analysis, increased data collection, and the development of more accurate and robust probabilistic analysis methods. Not including qualitative sources such as human error, we categorize the various sources of error as follows:

1. Model approximation
  - a. First or second-order approximation
  - b. Calculation of derivatives
2. Uncertainty characterization
  - a. Insufficient data
  - b. Selection of incorrect distribution
3. Numerical algorithm
  - a. Transformations to standard normal
  - b. Convergence error in finding the MPP
  - c. Algorithm error (wrong or multiple MPP)
4. Probability integration
  - a. Insufficient number of samples
  - b. First or second-order approximation

Model approximations are widely used to speed up the analysis when the original deterministic model is complex and/or computationally intensive to evaluate. First and second-order approximations to the original deterministic model are widely used. To construct these approximations, derivatives of the original model response are required, which if not carefully done, can be a major source of error. Deterministic (V&V) can be used *to reduce* model approximation error, whereas probabilistic analysis methods can be used *to assess* the effect of model approximations.

Probabilistic analysis requires a statistical characterization of the input variables. Therefore, estimation of the statistical moments will contain some associated uncertainty due to lack of data. This form of error is effectively modeled using a Bayesian approach where the inclusion of additional data can be shown to reduce the uncertainty in the statistical moments to zero as the amount of data approaches infinity.<sup>9</sup> Selection of the proper distribution can be difficult unless a fairly large amount of data or experience is available. Fortunately, sensitivity studies can be performed to determine which input distributions are important such that subsequent data collection efforts can be focused in the proper areas.

Numerical algorithms are required to locate the MPP for non-sampling probabilistic analysis techniques. Briefly, this a process of locating the minimum distance from the failure surface (subject to  $g=0$  in Figure 1) to the origin in standard normal ( $\mu=0, \sigma=1$ ) space.<sup>9</sup> One aspect of the process is the mapping of non-normal probability distributions to standard normal, which in many cases is performed numerically, and thus, will contain some element of error. Since optimization algorithms are used to locate this minimum distance point, iterative or stochastic sampling techniques are used introducing an additional source of error. Both the transformation to standard normal and optimization convergence error are reducible by the use of tighter convergence tolerances or more accurate numerical methods.

The third source of numerical algorithm error is arguably the most troublesome—the inability of the algorithm to locate the correct MPP. This can result for a variety of reasons such as locating a local minimum when a global minimum exists, the presence of multiple minimums, and violations of the assumptions of a smooth and continuous response surface. The challenging aspect of this error is that the problem may arise *after* transformation to the standard normal space. If the mapping from original to standard normal space is highly nonlinear, ill-behaved failure surfaces can be generated unbeknownst to the user. Although difficult to detect and treat in general, this form of error is correctly classified as reducible through the development of more robust numerical methods, error checking, and adaptive analysis strategies.

The last type of error arises in the calculation of the failure probability. For sampling methods, this error can be eliminated (in the limit) by increasing the number of samples. Again, although impractical to achieve, this form of error is reducible. For MPP-based methods, the probability integration will only be exact if the failure surface is modeled exactly in the transformed space, i.e., linear or quadratic, which is usually not the case. In many probabilistic methods,

first and second-order approximations are typically used. It should be noted that this failure surface approximation is in addition to the approximation made in representing the original numerical model. Again, this approximation is problematic since the user is generally unaware of the existence or magnitude of the error.

In general, when working with analytical models we recommend using Monte Carlo simulation. We apply MPP-based probabilistic methods to analytical models in this paper because well-behaved functions in x-space may not be well-behaved in u-space where the probability integration is performed. Thus, the analytical models used in this paper could easily have been complicated finite element models.

In the following example problems, the various sources of error discussed above are illustrated, and suggested approaches for their mitigation proposed. Since the focus of this paper is on the accuracy and robustness of modern probabilistic analysis methods, simple deterministic models are used such that important points could be more easily made and visualized without paying undue attention to the details of the deterministic model.

For all cases presented, the numerical calculations were performed using the current developmental version of the NESSUS computer software (Southwest Research Institute, Version 3). NESSUS is a general-purpose tool for computing the probabilistic response or reliability of engineering systems.<sup>8</sup> It was initially developed by a team led by SwRI for the National Aeronautics and Space Administration (NASA) to assess uncertainties in critical space shuttle main engine components.<sup>10</sup> NESSUS has since undergone and is undergoing significant enhancement.<sup>11</sup> The framework of NESSUS allows the user to link advanced probabilistic algorithms with analytical equations, external computer programs including commercial finite element codes, and general combinations of the two.

For locating the MPP, NESSUS uses a modified version of the standard RF method,<sup>8</sup> MMFD, SLP, or SQP. The modified RF method provides additional convergence checks in addition to the standard check for convergence of the safety index,  $\beta$ , that is,

$$\frac{|\beta_i - \beta_{i-1}|}{\beta_{i-1}} \leq 0.01 \quad (1)$$

NESSUS also checks for convergence on the response,  $Z$ , and that the angle between successive MPP's is within a user-specified tolerance, i.e.,

$$\frac{|Z_i - Z_{i-1}|}{Z_{i-1}} \leq 0.01 \quad (2)$$

and

$$\theta = \cos^{-1} \alpha_i \cdot \alpha_{i-1} \leq \varepsilon (= 30^\circ) \quad (3)$$

In NESSUS, the modified RF method is employed first since it is the most efficient. If convergence difficulties are encountered, the method is switched to SQP.

Unless otherwise noted, all Monte Carlo solutions presented were obtained using 100,000,000 samples. To reflect the approximate nature of the Monte Carlo solution itself, we also present the 95% confidence bound on the Monte Carlo solution. AMV+ solutions were obtained using a tolerance of 5%. AIS2 solutions were obtained using an allowable error of 5% with 95% confidence. Quality of fit for the RSM results, as measured by the standard  $r^2$  is noted in the respective figures.<sup>9</sup> Unless otherwise stated, a central composite (CC) design with move limits of  $2\sigma$  were used for the RSM.

### Example Problems

In the following sections, we present solutions to five example problems. For each problem, we apply FORM, SORM, AMV+, AIS2, RSM, and Monte Carlo. The computed cdf is reported as well as the percent error from the Monte Carlo solution. Where necessary, we also utilize contour plots to visualize the  $g=0$  surfaces in u-space and associated MPP locations. The Mathematica software (Wolfram Research, Version 3.0) was used to construct these visualizations from the analytical functions. Note that we have intentionally not reported efficiency or calculation time measures since the focus of this paper is on accuracy and errors.

#### Example 1 – Gear Contact Stress Model

This example was taken from the set of numerical review problems assembled by the Society of Automotive Engineers (SAE) G-11 Probabilistic Methods Committee of which the authors are active participants. The objective of the numerical review subcommittee is to assess the performance of several popular probabilistic methods. Researchers and practitioners from the probabilistic mechanics technical community contributed the problems, which were devised to expose weaknesses in traditional algorithms used in probabilistic analysis.

The response function for the gear contact stress response model is given in the Appendix. The model variables and their respective statistical inputs are listed in Table 1. Note that the response function is nonlinear and the input variables are all normally distributed.

A plot of the joint probability density function (jpdf) is shown in Figure 2 for the dominant random variables  $P_d$  and  $\sigma_N$ . Since all of the input variables are normally distributed, the mapping to standard normal is linear and no approximation is made. The jpdf shown in Figure 1 is rotationally symmetric about the origin and decays exponentially in the radial direction. These properties allow probabilities to be computed very easily assuming first or second-order intersections with the jpdf.

**Table 1. Input variables for Example 1.**

Var	Name	Mean	SD	Dist
$f$	Face width (in.)	0.5	0.025	Normal
$\phi$	Pressure angle (deg.)	20	1.0	Normal
$T_P$	Torque (lb-in)	108	5.4	Normal
$E$	Modulus of elasticity (ksi)	30000	1500	Normal
$P_d$	Diametral pitch (1/in.)	9	0.45	Normal
$\sigma_N$	Allowable surface pressure (ksi)	88	4.4	Normal
$N_1$	Number of teeth of the pinion	18	0.9	Normal
$\nu$	Poisson's ratio	0.25	0.0125	Normal
$m_g$	Gear ratio	3.78	-	-

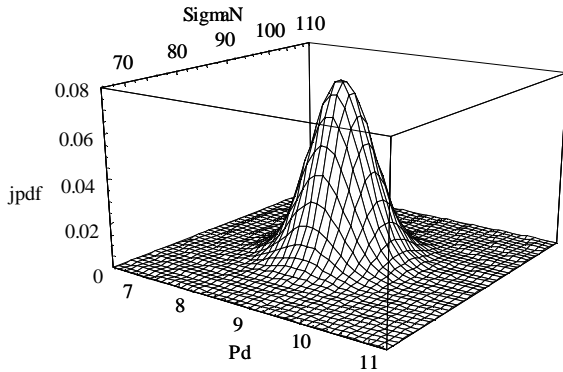


**Figure 2. Joint pdf for Example 1.**

The response for the two dominate random variables,  $P_d$  and  $\sigma_N$ , is well behaved and fairly linear in both the original x-space (Figure 3) and the transformed u-space (Figure 4). Since the transformation from normal to standard normal is linear, the two surfaces are identical. The similarity of the response surface in original and transformed space is shown here to contrast the difference in subsequent examples.

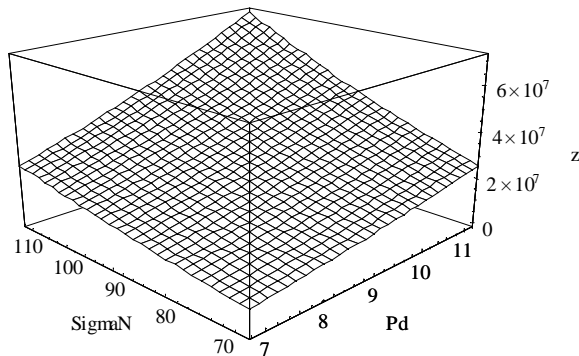


**Figure 3. Response surface for Example 1 for variables  $P_d$  and  $\sigma_N$ .**

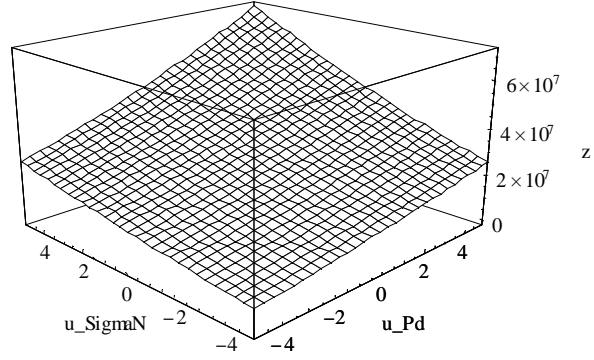


**Figure 4. Response surface for Example 1 for transformed (u-space) variables  $P_d$  and  $\sigma_N$ .**

Because this problem has eight random variables and the CC design in NESSUS is limited to seven random variables, the RSM solution for this problem was obtained by performing a fractional factorial design consisting of the minimum number of perturbations required to fit a full quadratic polynomial. Move limits were  $\pm 2\sigma$  on each random variable.

The computed cumulative distribution function (cdf) is shown in Figure 5 with probabilities on a standard normal scale (u). As shown, all methods performed exceptionally well, which is not unexpected given the mild non-linearity of the problem in the transformed space. The only exception is RSM solution, which has some error in the left tail of the cdf.

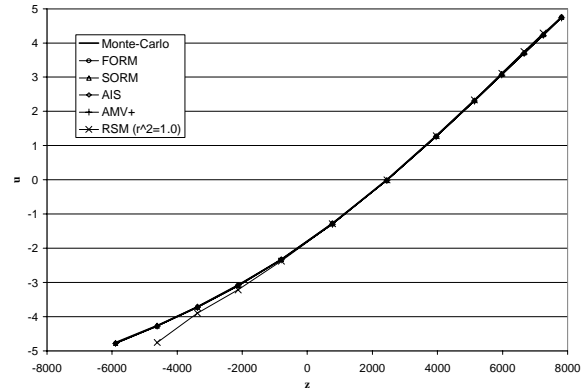


**Figure 5. Computed cumulative distribution function for Example 1.**

Because it is difficult to discern the error in the extreme tail regions in Figure 5, a plot of the percent error for the various methods is also presented in Figure 6. RSM results were not obtained for the leftmost point and rightmost two points in 10,000,000 simulations; therefore, no error is reported. The dashed line represents the 95% confidence bounds on the computed Monte Carlo solution. Although 95% is arbitrary, we feel it is unreasonable to expect non-Monte Carlo solutions to be any more accurate than these bounds.

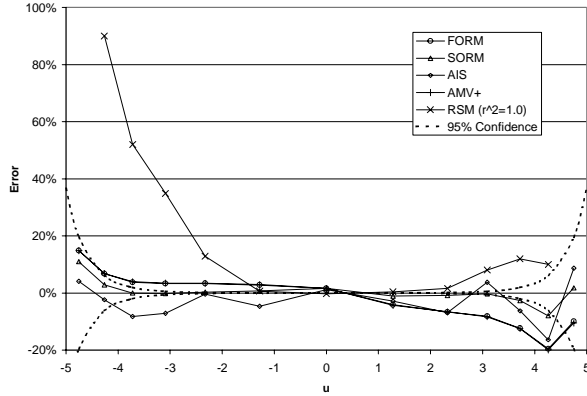


Figure 6. Solution error for Example 1.

The RSM had difficulty on this problem because of the accuracy of the fitted polynomial. As indicated, the quality of the fit was perfect ( $r^2=1.0$ ); however, this measure does not ensure the response surface is accurate at points outside of the fitted region, which is the case here.

This problem illustrates that excellent probability solutions can be obtained using efficient and accurate probabilistic methods provided numerical problems do not arise during the solution process. It also emphasizes the need to ensure the approximate model accurately represents the exact function—unless careful checking is performed on the fitted surface, accuracy can neither be measured nor guaranteed. Ref. 12 proposes some checks that can be performed for RSM.

### Example 2 – 1D Dynamic Oscillator Model

This problem considers the displacement response of a one-dimensional dynamic oscillator. The response function is given in the Appendix. Full details on the variables and development of the model can be found in Ref. 13. A plot of the displacement response vs. frequency ( $\omega$ ) is shown in Figure 7. The important point to note is that the response clearly violates an assumption inherent to MPP-based methods, which is that the response be smooth and continuous. Although the function is single valued, the presence of the discontinuity is likely to cause problems locating the MPP and error in the probability integration.

The results from the probabilistic analysis reported in Ref. 13 are shown in Table 2. FORM and SORM both had difficulty with several of the cases; AMV+ reported convergence for DOE Case 8, which clearly is in error.

Cruise<sup>13</sup> found that by rewriting the original response function into an inverse form, the problem was more tractable. The inverse relationship is given in the Appendix. As shown in Table 3, using the inverse form of the response function, AMV+, FORM and SORM all obtained excellent solutions compared to Monte Carlo.

Table 2. Probabilistic results for Example 2 using initial form of the response function.

DOE Case	N_sims	MC (TAC)	AMV+	FORM	SORM
2	600K	0.00017	0.00016	0.0000	$\sim 10^{-26}$
4	200K	0.00763	0.00764	$\sim 10^{-32}$	$\sim 10^{-42}$
6	600K	0.00059	0.00059	0.0000	0.0000
8	200K	0.01440	0.99980	$\sim 10^{-25}$	0.0000
10	600K	0.00369	0.00356	0.00309	0.0037
12	200K	0.03040	0.02940	0.99990	0.9999
14	200K	0.02448	0.02335	0.02200	0.0239
16	200K	0.08477	0.08210	0.07940	0.0834

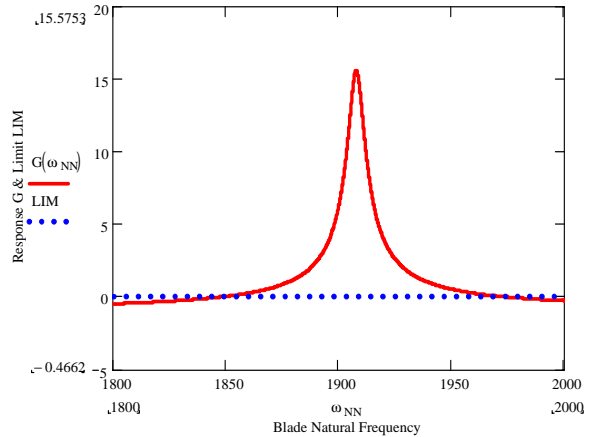


Figure 7. Displacement response of the 1D oscillator.

Table 3. Probabilistic results for Example 2 using the modified response function.

DOE Case	N_sims	MC (TAC)	AMV+	FORM	SORM
2	600K	0.00017	0.00016	0.00014	0.00016
4	200K	0.00756	0.00761	0.00738	0.00773
6	600K	0.00058	0.00059	0.00056	0.00060
8	200K	0.01456	0.01441	0.01419	0.01467
10	600K	0.00369	0.00354	0.00310	0.00364
12	200K	0.02920	0.02906	0.02751	0.02968
14	200K	0.02445	0.02338	0.02201	0.02381
16	200K	0.08401	0.08153	0.07946	0.08383

This example demonstrates that erroneous solutions can be obtained if the assumptions inherent to the methods being used are not met, namely that the response is smooth and continuous. In some situations, such as this example, the problem can be reformulated such that assumptions inherent to the method being used are not violated. As a minimum, it is recommended that software tools check assumptions before proceeding on with the analysis.

### Example 3: Low Cycle Fatigue Model

The response function is:

$$\log N = \frac{700}{\sigma} - 3 + \varepsilon \quad (4)$$

where  $N$  is the number of cycles,  $\sigma$  is the stress (ksi) having a mean of 95 and standard deviation of 5, and  $\varepsilon$  is the

regression model error having a mean of zero and standard deviation of 0.3. Both random variables are normally distributed.

The joint pdf is similar to that in Example 1, so it is not shown here. The computed cdf (right tail only) is shown in Figure 8. From the figure, it is clearly evident that the MV and AMV solutions are in error compared to the FORM, SORM, AIS, AMV+, and RSM solutions. The reason for this error can be explained with the aid of Figure 9, which shows the  $g=0$  limit states for all levels in the cdf shown in Figure 8 as well as the approximate and exact most probable point locus (MPPL). (The MPPL is constructed by joining successive MPP's.) Probabilistic solutions using the MV method are based on the approximate MPPL; therefore, the solution will only be accurate, in general, near the median response. The AMV solution attempts to correct the solution with a response update using the MPP information. If the difference between the MV and AMV solution is large, the AMV+ method is required, which as shown in Figure 8. As shown, there is excellent agreement between AMV+ and Monte Carlo.

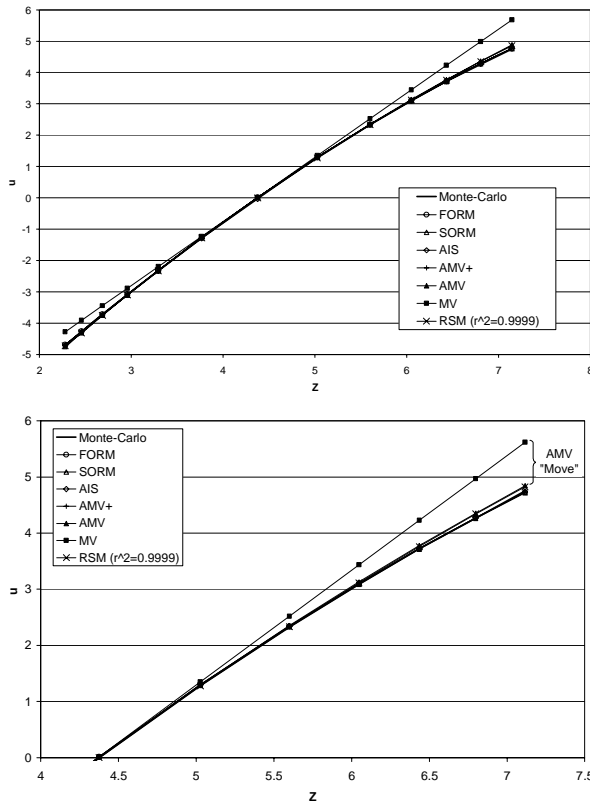


Figure 8 Full cdf and right tail cdf for Example 3.

A comparison of the error compared to Monte Carlo is shown in Figure 10. With the exception of MV, which did not perform well for reasons given above, all of the methods performed reasonably well. AMV and RSM are outside the 95% confidence limits, but do capture the correct trend and approximate probabilities.

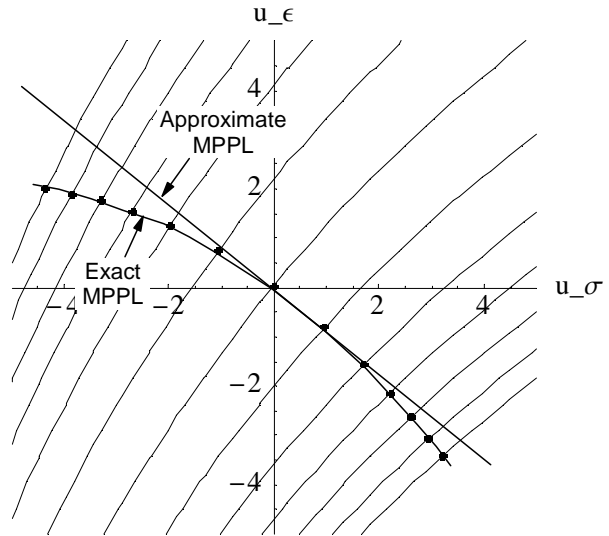


Figure 9. The  $g=0$  limit states, approximate MPPL, and exact MPPL for Example 3.

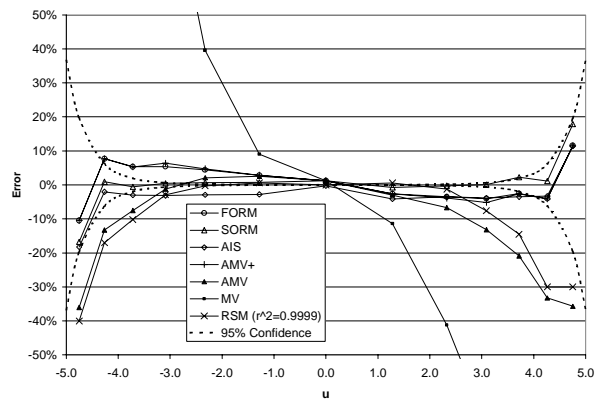


Figure 10. Solution error for Example 3.

This example illustrates the danger in using AMV solutions when the difference between MV and AMV is large, i.e., unconverged results. In this instance, iterations using AMV+ are required. Although this conclusion is intuitively obvious, the authors have observed AMV solutions being reported in the context of converged solutions when the difference between MV and AMV was clearly unacceptable.

**Example 4: Maximum Radial Stress of a Rotating Disk**

This problem considers the maximum radial stress in a rotating disk. The complete function is given in the Appendix. The input variables are listed in Table 4.

A key feature of this problem is the use of a uniformly distributed random variable for the rotor speed. The joint pdf in terms of the two dominate random variables, rotor speed and outer radius, is shown in Figure 11. As shown, the joint

pdf is bounded in one direction and normally distributed in the other.

**Table 4. Input variables for Example 4.**

Var	Name	Mean	SD	Dist
$\nu$	Poisson's Ratio	0.30	0.005	Normal
$\rho$	Density (lb/in <sup>3</sup> )	0.284	0.002	Normal
$\omega$	Rotor Speed (rpm)	10500	288.7	Uniform (10000, 11000)
$r_o$	Outer Radius (in)	8	0.02	Normal
$r_i$	Inner Radius (in)	2	0.01	Normal

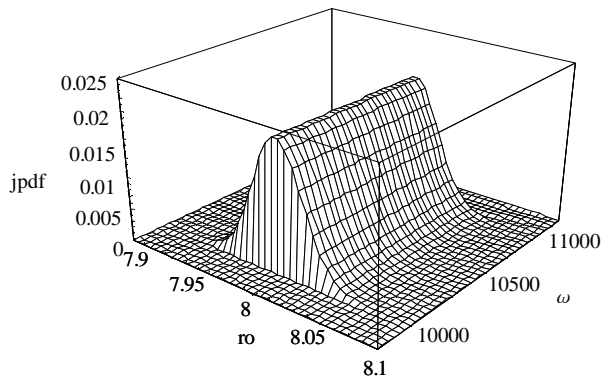


**Figure 11. Joint pdf for Example 4.**

The effect of the uniform distribution on the mapping from  $x$  to  $u$ -space can be seen by comparing the response surface in original ( $x$ ) space, shown in Figure 12, with the response surface in transformed ( $u$ ) space, shown in Figure 13. As shown, an otherwise well-behaved response surface in  $x$ -space is transformed to a highly nonlinear response surface in  $u$ -space.

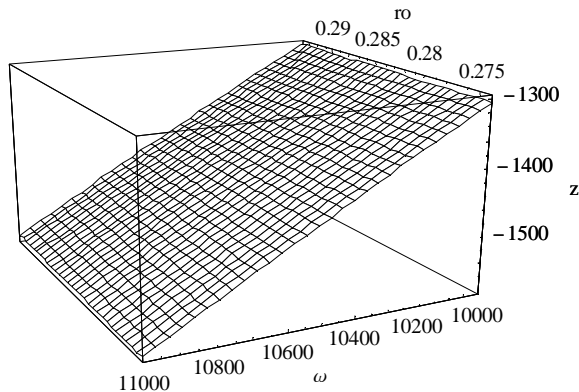


**Figure 12. Response surface in original ( $x$ ) space for Example 4.**

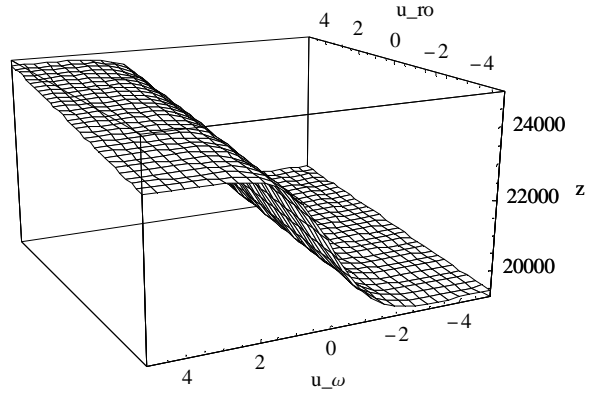


**Figure 13. Response surface in transformed ( $u$ ) space for Example 4.**

The  $g=0$  contours for several different levels are shown in Figure 14. For this problem, the modified RF optimization algorithm fails to converge to the correct MPP for all but four levels, but numerous warning messages were issued signaling a problem. Consequently, the SQP optimizer was selected within NESSUS and the correct MPP's (shown as black markers in Figure 14) located for all levels. Plotting only two variables out of 5 causes the MPP markers to appear slightly off the limit states; however, the  $g=0$  conditions is met.

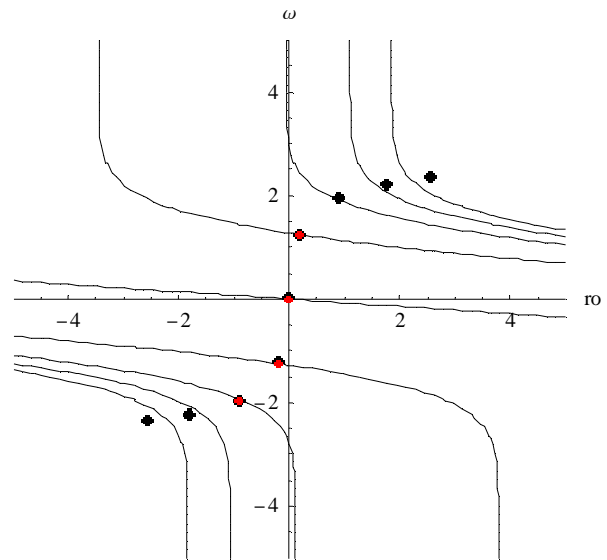


**Figure 14. Several  $g=0$  limit states and corresponding MPP's located using SQP in NESSUS.**

The computed cdf for Example 4 is shown in Figure 15 (full cdf, left tail, and right tail). As shown, all methods perform reasonably well near the median where the response is smooth. However, in the tail regions FORM and AMV+ are in error, whereas SORM, AIS2, and RSM all agree with Monte Carlo very well. SORM and AIS2 perform well because the second order approximation in  $u$ -space works well for this example. RSM performs well because the response surface is fit in the original space (Figure 12) and not in the transformed space.

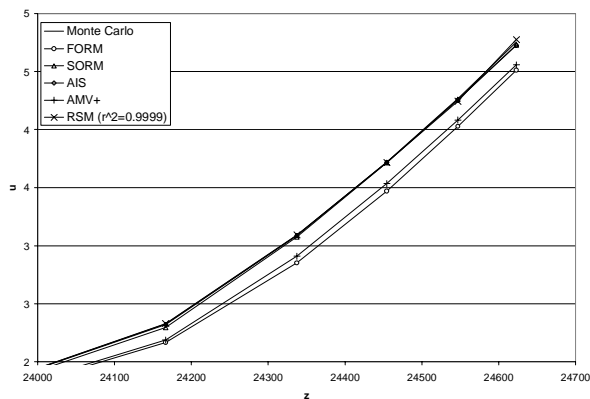
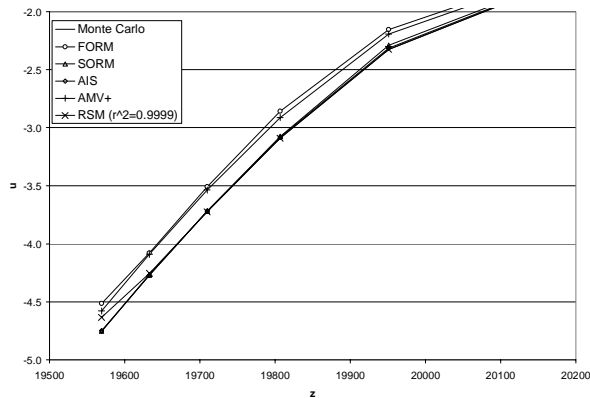
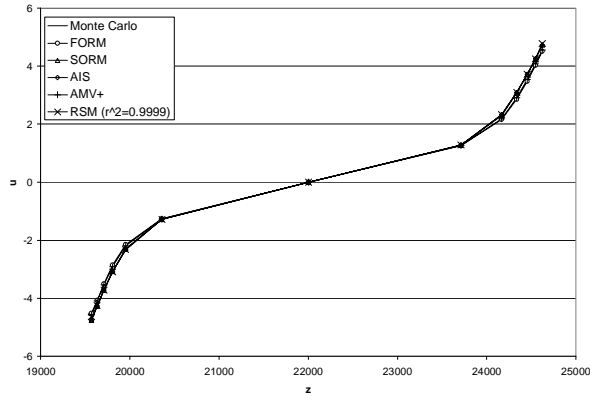


Figure 15. Computed cdf for Example 4.

The reason that the FORM and AMV+ solutions contain some error is because both assume a first-order function in u-space, which is inaccurate in this Example. This source of this error, shown in Figure 16, can be understood with the aid of Figure 14. A first-order approximation to the  $g=0$  surface at the MPP's near the origin is reasonably accurate because the failure surface is fairly flat. Further out in the tail regions, however, the  $g=0$  surface is more accurately approximated with a quadratic. (The AMV+ solution could be improved by using a second order approximation)

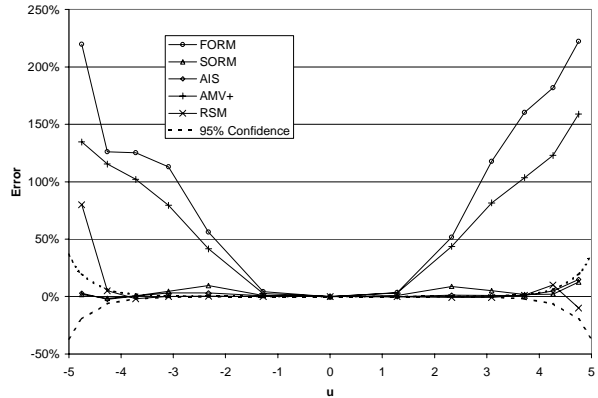


Figure 16. Solution error for Example 4.

This example illustrates the need for robust optimization methods that can locate an MPP in difficult situations. Also, once the MPP has been confidently identified, the computed probability must be checked, either by application of independent methods or by adaptive sampling.

It is also important to note that the original response surface is well-behaved in terms of the input variables. It was the transformation into u-space that challenged several of the probabilistic methods. Thus, the user must be careful to understand not only the physics of the problem, but also the ramifications of using a probabilistic method that performs calculations in a transformed space.

### Example 5: Multiple MPP Problem

The response function for Example 5 is:

$$Z = 3 + 2X_1^4 - X_1^2 - X_2 \quad (5)$$

where both  $X_1$  and  $X_2$  are standard normal random variables. The response surface in transformed space is shown in Figure 17 (the surface in original space is the same).

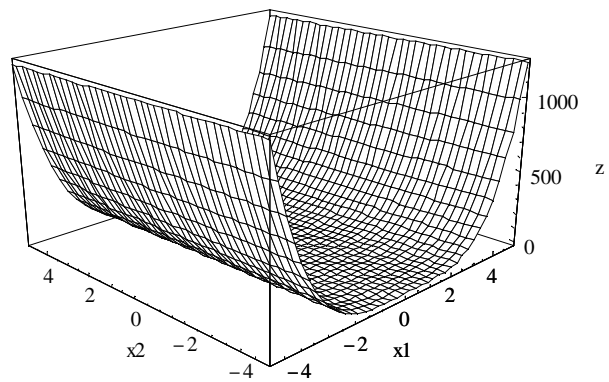


Figure 17. Response surface in u-space for Example 5.

Examining the response function, we see that it is symmetric with respect to  $X_1$ . Thus, if an MPP exists where  $X_1 \neq 0$ , then two MPP's actually exist, located at  $\{-X_1^*, +X_2^*\}$  and  $\{+X_1^*, +X_2^*\}$ .

The  $g=0$  surfaces for 13 different response levels are shown in Figure 18. The modified RF method failed to converge on most levels; thus, the MPP's were found using SQP and are delineated with black markers in Figure 18. Even using SQP, however, the multiple MPP condition clearly evident in Figure 18 was not detected and only one of two MPP's at any given level was found. In Figure 18, the MPP's are numbered in ascending order right moving from low probability (left tail) to high probability (right-tail).

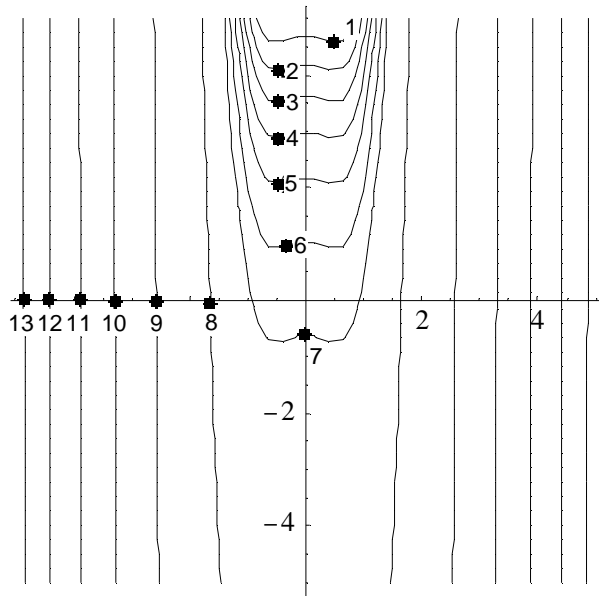


Figure 18. Limit states and MPP's for Example 5.

AMV+ and FORM, both using the modified RF optimizer, reported convergence problems. However, after switching to the SQP optimizer, no warnings were reported and convergence was obtained, but to only one of the two possible MPP's. In this instance, the lack of convergence information reported by the modified RF optimizer was useful in detecting the multiple MPP condition.

Obviously, incorrect results will be obtained if the probability integration is performed based on only one MPP at any given level when multiple MPP's exist. However, for the purposes of comparing probabilistic methods and errors, cdf results are reported based on the converged MPP's shown in Figure 18.

The cdf is shown in Figure 19 (top: full cdf, middle: left tail, bottom: zoomed view of central portion). The near vertical condition in the lower left tail shown in the upper figure can be more clearly seen in the middle figure and the central region can be more clearly seen in the lower figure. The levels are numbered in the middle and lower plots in Figure 19 and correspond to the MPP's numbered in Figure 18.

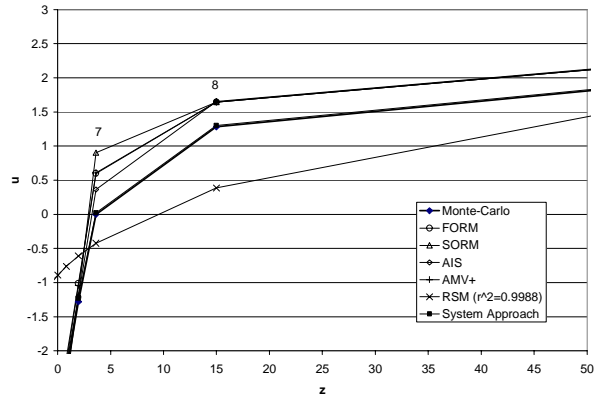
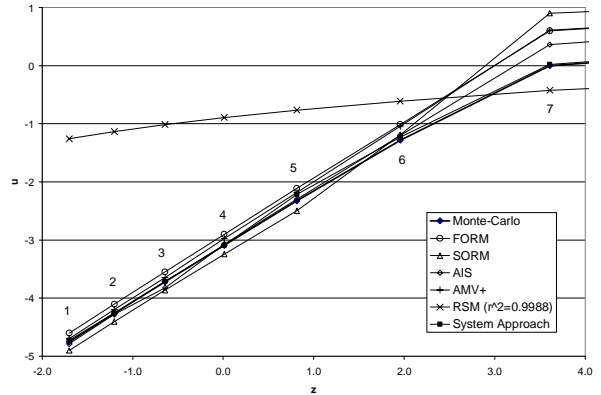
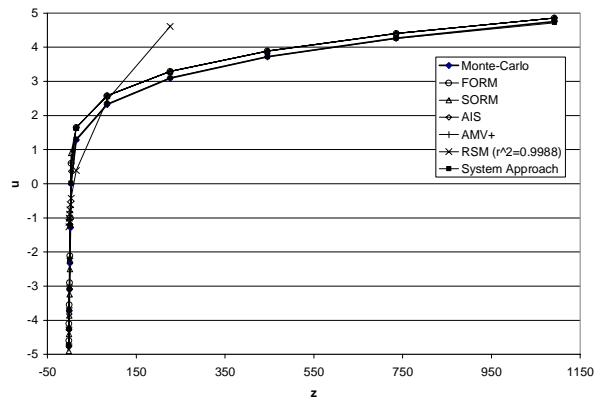


Figure 19. Computed cdf for Example 5 (top: full cdf, middle: left tail, bottom: zoomed view of central portion).

As shown, The RSM performed very poorly on this problem because the original 4<sup>th</sup> order function is not approximated accurately with the full quadratic used in the CC response surface design. Using wider move limits, e.g.,  $\pm 3\sigma$  and  $\pm 4\sigma$ , improved the quality in the extreme regions, but at the expense of the quality in the central region.

The other methods appear to have performed reasonably well in the left tail region (points 1-6), but more poorly at level 7. This is because the two MPP's at each level are relatively close to each other, and because a first and second-order approximation at one MPP captures the majority of the jpdf in

the  $g \leq 0$  region. At level 7, where there is a single MPP along the  $X_I=0$  axis, the error is greater because the curvature is not approximated as well and because the “cupped” regions become more pronounced (missed probability).

As shown in Figure 20, all methods reported close but slightly different solutions at levels 1-7 owing to their differences in calculation method and approximations (the levels correspond to the points on each curve and are numbered in consecutive order moving from left to right). Figure 20 also reveals that the error in the left tail results is quite significant. At levels 8-13, where there are two MPP’s that are not close together, all of the methods (except Monte Carlo) computed cdf values that are in error. This error is due to only one MPP being used.

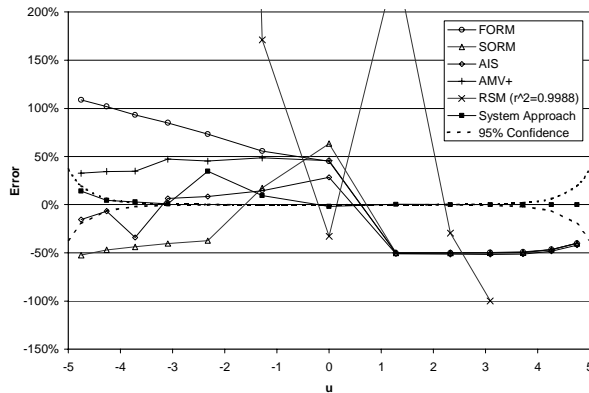


Figure 20. Normalized errors for Example 5.

This example illustrates the need for methods that can detect multiple MPP’s. Given the existence and detection of multiple MPP’s, an analysis strategy that can accurately compute probabilities in this situation is needed. Such a strategy is discussed in the next section.

**Proposed Strategy: System Approach**

An approach is proposed that uses a sampling technique to locate all MPP’s for a given level. Once all MPP’s are located, a system approach where the problem is divided into multiple g-functions is proposed.

**Sampling Based MPP Search**

Sampling may be effectively used to estimate MPP’s in the transformed space because analytical functions are used. Other researchers have also proposed other techniques to deal with multiple MPP’s.<sup>14</sup> Here, we give an example using Monte Carlo sampling to estimate the MPP’s; however, other more efficient sampling methods could also be used.

The procedure for estimating the MPP’s using Monte Carlo sampling is straightforward:

1. Estimate the probability of failure using sampling,
2. Convert the realizations in the failure region to u-space
3. Evaluate the distance to the origin for each realization,

4. Sort the results and report the realizations with the shortest distance. (other information such as the u-space and x-space values are also reported)

The drawback to this approach is that, first, the number of samples to estimate the MPP may be extremely large and therefore costly even for fast running analytical g-functions, and second, it may be difficult to distinguish true multiple MPP’s using random sampling. However, a sampling based approach may be practical when analyzing an approximating function to a complex problem, e.g., a linear, quadratic, or response surface of a finite element model.

To demonstrate, a simple sampling based MPP search routine was implemented in NESSUS. Example 5 was run and 1899 failure points from a 2,000,000 sample Monte Carlo analysis were used to estimate the MPP locations. The sample results were sorted and the angle between the sample point of minimum distance and successive points computed. These results are shown in Table 5 and plotted in Figure 21 for the ten samples with the shortest distance to the origin in u-space. The results clearly indicate the existence of two MPP’s.

Table 5. Results from the sampling based MPP search.

Sample No.	Angle (degrees)	Beta
1	0.00	2.915
2	18.50	2.918
3	17.00	2.918
4	17.80	2.920
5	19.10	2.921
6	17.90	2.921
7	17.50	2.921
8	0.80	2.923
9	0.70	2.925
10	1.50	2.925

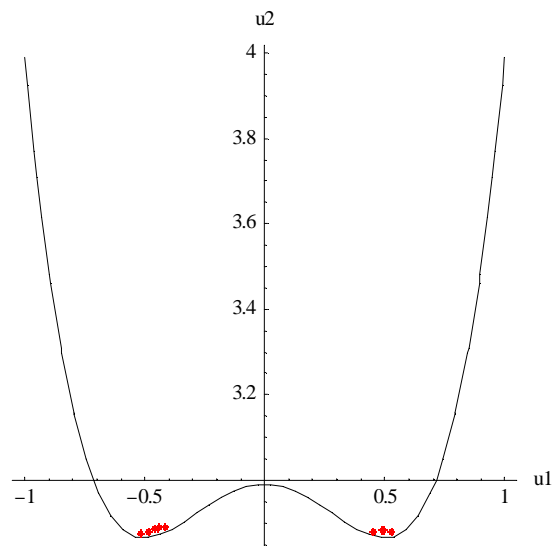


Figure 21. Limit state and MC MPP samples estimates.

## System Analysis

Once all MPP's are found, the problem can be subdivided and solved using a system analysis. A system analysis consists of approximating the limit state at each MPP and using a probabilistic fault tree<sup>15</sup> to compute the system probability.

NESSUS has a system analysis capability that has been demonstrated on numerous problems.<sup>15</sup> Using the multiple MPP information, a system analysis was performed at each of the 13 levels for Example 5. As shown in Figure 19 and Figure 20, the computed results—labeled “system approach”—are in excellent agreement with the Monte Carlo solution. Thus, although not automated in software tools like NESSUS yet, this approach shows promise for difficult problems like Example 5.

## Conclusions and recommendations

In this paper we address the issue of errors in probabilistic analysis. We differentiate uncertainties, which are inherent or are statistical variations in input parameters, from errors, which are deterministic in nature. Errors can be reduced through verification and validation, increased data collection efforts, and the development of more accurate and robust probabilistic analysis methods. Through several example problems that were devised to challenge modern probabilistic methods, we illustrate many of the pitfalls inherent to currently used probabilistic analysis methods.

NESSUS was used to compute solutions to all of the SAE numerical review test cases; only a subset consisting of the more challenging problems were presented here. The fact that knowledgeable and trained analysts were required to obtain quality solutions evidences the concern that many adopters of probabilistic technology are currently expressing—that further research and development of robust methods are needed before probabilistic technology will be integrated into the current design cycle. Although we agree with this concern, we also note that fully robust (fail-safe) methods that can handle large complex problems will be difficult, if not impossible, to develop. Like verification and validation, achieving robustness is a process and not a product. Consequently, probabilistic technology will be integrated into design when the gap between robust analysis tools and user knowledge and training in the use of probabilistic methods decreases to an acceptable level.

An important point to note is that the NESSUS implementation of the advanced mean value (AMV+) method and the modified RF optimizer were the only methods out of all evaluated that identified when problems were occurring. Thus, although the AMV+ and modified RF method do not currently automatically adapt and correct when problems occur, they at least warn that convergence is not reached or that non-monotonic behavior is detected. This is obviously the first step in adapting to a more robust analysis strategy such as the proposed system approach.

A large number of probabilistic analysis methods and several optimization techniques are available in NESSUS making it a

very general and powerful tool for performing probabilistic analysis. The current need for probabilistic technology to support critical applications such as certification by analysis requires confidence in the generated solutions. This will come only after robust methodologies are demonstrated on small devised problems as well as on large-scale high-fidelity problems. Therefore, it is recommended that robust probabilistic methods be developed that have the ability to recognize when numerical problems are occurring and adjust or adapt to either a different solution strategy.

## Acknowledgements

The authors would like to recognize the outstanding effort of Ms. Jill O'Keefe for her assistance with the calculations and plotting. The authors also acknowledge the support of the SwRI Advisory Committee for Research, Project 09240.

## References

1. Oberkampf, W.L. *et al.*, “Estimation of Total Uncertainty in Modeling and Simulation,” SAND2000 – 0824, Sandia National Laboratory, April 2000.
2. Madsen, H. O., Krenk, S., and Lind, N. C., Methods of Structural Safety, Prentice-Hall, Inc., New Jersey, 1986
3. Y.-T. Wu, H. R. Millwater, T. A. Cruse, “Advanced Probabilistic Structural Analysis Methods for Implicit Performance Functions,” *AIAA Journal*, 28(9), 1990.
4. Faravelli, L., “Response Surface Approach for Reliability Analysis,” *J. of Eng. Mech.*, 115(12), 1989.
5. Y.-T. Wu, “Computational Method for Efficient Structural Reliability and Reliability Sensitivity Analysis,” *AIAA Journal*, Vol. 32, 1994.
6. Vanderplaats, G.N., Numerical Optimization Techniques for Engineering Design, McGraw-Hill, Inc., 1984
7. Rackwitz, R. and Feissler, B., “Structural Reliability Under Combined Random Load Sequences,” *Computers and Structures*, 9(5), 1978.
8. Southwest Research Institute, NESSUS Reference Manual, Version 2.4, 1998.
9. Ang, A. H.-S. and Tang, W. H., 1984, Probabilistic Concepts in Engineering Planning and Design, Volume II: Decision, Risk, and Reliability, New York: John Wiley & Sons, Inc.
10. Southwest Research Institute, “Probabilistic Structural Analysis Methods (PSAM) for Select Space Propulsion System Components,” *Final Report NASA Contract NAS3-24389*, NASA Lewis Research Center, 1995.
11. Riha, D. S., Thacker, B. H., Millwater, H. R., Wu, Y.-T. and Enright, M. P., “Probabilistic Engineering Analysis Using the NESSUS Software,” *Proc. 41<sup>st</sup> Structures, Structural Dynamics, and Materials Conf.*, Atlanta, Georgia, 3-6 April 2000.
12. Fox, E.P., “Issues in Utilizing Response Surface Methodologies for Accurate Probabilistic Design,” *Proc. 37<sup>th</sup> Structures, Structural Dynamics, and Materials Conf.*, AIAA-96-1496, April 1996.
13. Cruse, T.A., “Issues and Strategies in Probabilistic Structural Modeling,” *Proc. 6<sup>th</sup> National Turbine Engine High Cycle Fatigue Conference*, 5-8 March 2001.
14. Der Kiureghian, A. and Dakessian T., “Multiple Design Points in First and Second-Order Reliability,” *Structural Safety*, 20, pg. 37-49, 1998.
15. Torng, T.Y., Wu, Y.-T., and Millwater, H.R., “Structural System Reliability Calculation Using a Probabilistic Fault Tree Analysis Method,” *Proc. 33<sup>rd</sup> Structures, Structural Dynamics, and Materials Conf.*, April 1992.

## Appendix – Example problem Response Functions

### Example 1 – Gear Contact Stress Model

$$Z = \sigma_N^2 \frac{2T_p E P_d^3 \sin \phi}{(1 - \nu^2) \pi \lambda N_1^3 \theta_1 \cos^2 \phi \left[ \sin \phi - \frac{\theta_1 \cos \phi}{(m_g + 1)} \right]} \quad (6)$$

where

$$\theta_1 = \text{Rollangle} = \frac{2 \left\{ \sqrt{\left( \frac{N_1 \sin \phi}{2} \right)^2 + N_1 + 1 - \pi \cos \phi} \right\}}{N_1 \cos \phi} \quad (7)$$

and

$$\lambda = f \frac{P_d}{N_1}$$

### Example 2 – 1D Dynamic Oscillator Model

$$\frac{LF \cdot MSF \cdot D_{nom} \left( \frac{Y}{100} \right) \left( \frac{\rho_{AllowNom}}{\rho_{Allow}} \right)}{\sqrt{\left[ 1 - \left[ \frac{m \cdot N / 60}{\omega_{NN} + S(N - N_{nom})} \right]^2 \right]^2 + \left[ 2\xi \frac{m \cdot N / 60}{\omega_{NN} + S(N - N_{nom})} \right]^2}} = 1 \quad (8)$$

Re-cast into inverse form yields

$$\frac{D_{nom}}{LF \cdot MSF} \left( \frac{\rho_{AllowNom}}{\rho_{Allow}} \right) \left( \frac{100}{Y} \right) \sqrt{\left[ 1 - \left[ \frac{m \cdot N / 60}{\omega_{NN} + S(N - N_{nom})} \right]^2 \right]^2 + \left[ 2\xi \frac{m \cdot N / 60}{\omega_{NN} + S(N - N_{nom})} \right]^2} + 1 = 0 \quad (9)$$

### Example 4: Maximum Radial Stress of a Rotating Disk

$$(\sigma_r)_{\max} = \left( \frac{3 + \nu}{8} \right) \left( \frac{\rho}{(9.81)(39.37)} \right) \left( \omega \frac{2\pi}{60} \right)^2 (r_o^2 - r_i^2) \quad (10)$$